

# A comparative Analysis and Optimization of two Supersonic Hybrid Solid Oxide Fuel Cell and Turbine-less Jet Engine Propulsion Systems for Unmanned Aerial Vehicles

M. Rostami<sup>1</sup>, A.H. Farajollahi\*, M. Marefati, R. Fili and F. Bagherpor

*Department of Aerospace Engineering, Faculty of Engineering, Imam Ali University, Kargar Street, Tehran, Iran.*

Received Date 05 September 2021; Revised Date 20 October 2021; Accepted Date 02 March 2022

\*Corresponding author: a.farajollahi@sharif.edu (A. Farajollahi)

## Abstract

The propulsion system of an Unmanned Aerial Vehicle (UAV) plays an essential role in its performance, stability, and flight endurance. In this work, two types of propulsion systems for UAVs (differentiated based on the fuel type) are studied in order to determine their characteristics and advantages. These proposed propulsion systems use a solid oxide fuel cell (SOFC) to generate the heat required for the operation of the turbine and generate thrust. In order to achieve the best operating condition, a multi-objective Non-Dominated Sorting Genetic Algorithm (NSGA-II) in MATLAB is used to decide the key design parameters. To reach the best conditions where the acceptable thrust is accompanied by a reasonable flight duration, the TOPSIS decision-making method is considered. The results obtained indicate that the efficiency and generated power of the propulsion system increase with a higher flight altitude or compressor pressure ratio. Also due to the recirculation of fuel in the SOFC's anode, a higher efficiency is observed in comparison to when hydrogen is used since anode-recirculation causes a higher fuel utilization. The optimization result shows that the efficiency and fuel consumption for the hydrogen-fueled system is 48.7% and 0.0024g/s, respectively, and 67.9% and 0.0066kg/s for a methane-fueled engine. It is also found that the maximum efficiency for both the hydrogen- and methane-fueled systems are available with the stack temperature of 1025 K; however the maximum thrust for these systems is at the stack temperature of 1075 K. In addition, increasing the fuel rate of the SOFC power unit helps the process of generating extra power and thrust for UAVs.

**Keywords:** UAV; SOFC Fuel Cell; Turbine-Less Jet Engine; Supersonic; Multi-Objective

## 1. Introduction

The solid oxide fuel cells (SOFCs) facilitated with a considerable capability of conserving energy have been investigated from different aspects as the experimental study cases and numerical simulation attempts [1-3]. As an innovative power source for portable application in vehicles, SOFCs have been subjected to many analyses incorporated with many commercial projects [4, 5]. STALKER-XE as a SOFC-powered unmanned aerial vehicle (UAV) has been experimentally applied by the Advanced Research Projects Agency [6]. They concluded considerable endurance for UAVs with the SOFC power resource in comparison with the battery-powered one. The process of production and testing of diesel heavy-duty trucks using SOFCs as an auxiliary power unit (APU) has been investigated [7]. Their results introduced SOFC APU as an important facility in the body of the power

generation system in their truck. Analyzing and designing different types of high-altitude and long-endurance UAVs that are capable of operating at different missions like surveying and inspections have mainly been subjected to many types of research works [8]. Over the past years, the aviation technology scientists became interested in publicizing the operation of the UAV propulsion system [9]. The gas turbine hybrid engines that utilize SOFCs have such a good propulsion capacity that can help electric UAVs to attain long endurance and high efficiency [10, 11]. The turbine-less hybrid propulsion system that contains a SOFC is known as a high effective performance equipment in the body of UAVs [12, 13].

In the past several years, many attempts have been made to numerous pieces of research works about the capability of combining SOFCs and gas

turbines[14, 15]. The hybrid systems that include SOFCs and gas turbines can be applied in aircrafts as the propulsion and electric generation sources [16, 17]. Himansu et al. [18] have concluded that the hydrogen-fueled gas turbine hybrid propulsion systems coupled with SOFCs can have a much higher efficiency in comparison to the internal combustion engines so that the hybrid one can be applied for HALE UAVs for long-duration missions between 10 to 20 days. According to Aguire et al. [19], the efficiency of the SOFC gas turbine hybrid system can be evaluated up to 66.3% for the case of SOFC with three stacks in the hybrid system configuration. Fernandes et al.[20]have realized that due to a considerable decrease of entropy in the process of hydrogen preheating, it cannot be a suitable fuel for aircrafts. The results obtained showed that the SOFC/gas turbine (GT) system provides are markedly higher exergy efficiency when compared to the other conventional competing propulsion systems. Okai et al. [21, 22]have found out that a hybrid system can operate as the main power source for distributed propulsion aircrafts due to their considerable efficiency of electric generation. Yanovski et al. [23] have shown that in the SOFC/GT hybrid systems, the high efficiency is in the case of using liquefied natural gas or liquid hydrogen. The fundamental complementary investigations have been included in many analyzes of SOFC/GT hybrid systems like thermodynamics investigations and safety operations [24-26]. Entirely, not so many investigations can be found about generating propulsive power by the gas turbine hybrid systems that contain SOFCs. Corresponding to Jansen et al. [27], the main factors of the aircraft propulsion system are specific power and efficiency. Bryce et al. [28]have confirmed that the propulsion systems of hybrid gas turbine that contain a fuel cell owe rarely low energy and power necessities, which are approximately not affected by the volume and weight of the propulsion system. UAVs that are suitable for high-altitude and long-endurance (HALE) missions, light aircraft, etc. are kinds of equipment that are proper for these applications. Ly et al.[29] have offered the idea of turbine-less jet engines due to the difficult adjustment of the combustion chamber outlet temperature that is the result of turbine blade material thermal properties. They proposed their analysis toward simulation and experiment of the turbine-less jet engine operation. Buchanan et al. [30] have applied the computational fluid dynamics method besides experimental tests in order to approach the results

that include a higher efficiency and operation cost reduction of turbine-less jet engines in comparison to the jet engines.

The capacity of SOFCs in working at high temperatures makes them beneficial in coupling with gas turbines. Accordingly, they can be best-fitted pieces of equipment for operating beside turbine-less jet engines. Regardless of innovation in the thermodynamics cycle structure of turbine-less jet engines, there are some obstacles that are the output of battery-powered compressors that can decrease the total efficiency of the system. Due to the large volume of the battery, the ratio of power and weight is lower compared to fuel. Being over-weighted for turbine-less jet engines is the consequence of increasing the battery power, thus utilizing these kinds of engines for long endurance operations cannot be done. Furthermore, a fixed amount of battery-powered UAVs weight during the commission concludes the decrease in efficiency that is the main challenge of supplying electric power for their compressors in a case of being turbine-less. By comparing the specific power of the conventional turbojet engines with turbine-less jet engines, the superiority of the turbine-less ones has been concluded obviously, and that is due to the replacement of turbines by motors. SOFCs have the capacity of generating a remarkable amount of electric power for consumption in motors. In addition, the outlet temperature of SOFCs can be high enough to be used by the nozzle in the engine. Operating as the high-speed flight for SOFC/GTs is a challenging issue that has been not investigated as much as thermal efficiency and fuel consumption in the previous publications of the aviation industry researchers. Although there are many kinds of research works investigating the operational characteristics, strong points and drawbacks of the combined propulsion system of SOFCs, and turbine-less jet engines, there is very little investigation regarding UAVs that fly in the supersonic conditions. The aim of this paper is to compare two different types of propulsion systems for a UAV flying at Mach 1.8, which use two different types of fuels. In addition, in the present paper, the effects of various factors such as altitudes and key design parameters of the propulsion system on the efficiency and flight duration are investigated. A comprehensive study to evaluate the performance of a SOFC-based propulsion system that considers the effects of various parameters on the performance of UAVs has not been observed in the literature. In addition, the results provided in this paper do not correspond to the results reported in the literature.

## 2. System description

Figure 1 indicates a schematic diagram of the SOFC turbine-less jet engines, with hydrogen and methane as the fuels. The SOFC jet engine can operate preferably in comparison to the turbojet engine due to a higher specific thrust and thermal efficiency that is due to the higher temperature of the exhaust gasses from the engine compared to the turbojet engines. Here is how the thermodynamic cycle generally operates. Initially, the intake and compressor boost the air pressure and temperature in the first and second stages of the process. Thereafter, hydrogen and hot air are supplied for the anode and cathode of SOFCs. Then the outlet streams from SOFCs mix with extra fuel in the combustor to burn the unused fuel in SOFCs and also adjust the inlet temperature of the nozzle. At the end, hot air after heating the inlet air of SOFCs enters the nozzle to be expanded, and generates the propulsion power for the UAV. The difference of the two cycles with different fuels is compared with each other in figure 1. Figure 1(a) indicates a diagram of the

hydrogen-fueled SOFC jet engine. In the hydrogen-fueled system, two heat exchangers are used due to the considerably low temperature of liquid hydrogen and the limitation of the pinch point of the heat exchangers. Figure 1(b) indicates a diagram of the methane-fueled SOFC jet engine. The high-pressure air is divided and applied in the reformer and cathode. There exists steam in the exhaust of the anode outlet that can be utilized by the reformer.

Two conventional fuels, the cryogenic liquid hydrogen and the cryogenic liquid methane were analyzed in the proposed cycles. Using hydrogen and methane as the fuel of SOFCs has some drawbacks like low volume energy density and difficult conditions of preparing low temperatures to liquefy them. However, the numerous investigations in the development of technology can provide the capability of applying hydrogen and methane as the fuel for power units in different kinds of vehicles like UAVs.

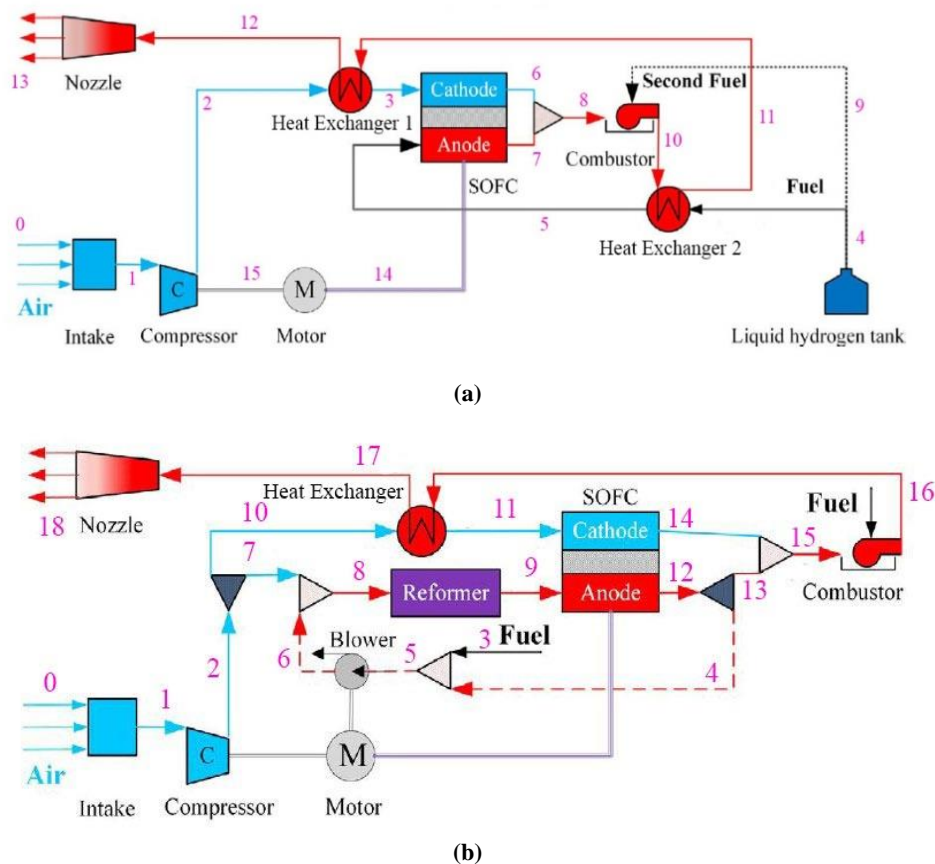


Figure 1. Schematic diagram of two hybrid SOFC and turbine-less jet engines with different fuels (a) hydrogen (b) methane.

### 3. Mathematical model

#### 3.1. Analysis assumption of simulation

In order to simplify the process of simulating the proposed propulsion system, several assumptions were made, which are listed as follow [31, 32]:

- The power unit system performance was considered steady-state.
- All the power unit elements were adiabatic.
- The air was composed of 21% oxygen and 79% nitrogen.
- The operational temperature of the fluids in the cathode and anode was the same.
- The operating gaseous fluids were assumed to behave as the ideal gases.

#### 3.2. Reformer model

The auto-thermal reforming reaction that is incomplete oxidation of the fuel takes place in the reformer and heat the air. The compressor provides the required oxygen, and the steam can be available from the anode output exhaust. Since the partial oxidation reforming reaction happens so fast, this reaction is assumed to be in an equilibrium state[33]. The temperature of the reformer outlet is expected to remain constant and equal to the reforming temperature. Note that the effect of the reforming temperature is not stated in

the results. The amount of oxygen to fuel ratio and reforming reaction heat are defined as equations 1 and 2 in table 1, respectively.

Table 1.Reformer’s mathematical model equations[34, 35].

Components	Equations	No.
Oxygen-fuel ratio	$R_{ref} = n_{O_2} / (n_{CH_4})$	1
Energy balance equation	$\Delta h_{ref} = h_{ref,out} - h_{ref,in}$	2

#### 3.3. SOFC model

A SOFC model for thermodynamic analysis is proposed in [36, 37]. According to the proposed propulsion systems, two different types of fuel can be used in SOFCs. Based on the fuel, some additional equipment may be required in the system. Since the methane fuel needs to reform the methane to hydrogen in order to be used in the fuel cell, many additional equations should be solved to simulate the process of converting methane to hydrogen. Besides, in this system, the anode recirculation loops to maximize the fuel utilization inside SOFCs, which further adds to the complexity of the system[38, 39]. The outlet gases of the reformer in the methane-fueled cycle are directed in to the anode section of the fuel cell. The reactions that take place in the reformer cooperate with the temperature increase of the flowing fluid in the stack; the reactions are as follow:

Table 2.Equations for SOFC mathematical model[34, 40].

Component	Equation	No.
Heat of electrochemical reaction	$Q_{elec} = T_{cell} \cdot \Delta S - j \cdot (\eta_{ohmi} + \eta_{conc} + \eta_{acti,anode} + \eta_{acti,cathode})$	3
Water gas phase transformation reaction	$CO + H_2O \leftrightarrow CO_2 + H_2 Q_{sh}$	4
Fuel cell equation of mass balance	$M_{i,in} + \sum_k C_{i,k} \tau_k = M_{i,out}$	5
Equation of energy balance in fuel cell	$\sum_i m_{i,in} c_{p,i} T_{in} - W_{out} = \sum_j m_{j,out} c_{p,j} T_{cell}$	6

The reaction of electrochemistry in the stack takes place at the three-phase boundary of the electrode, and the operational pressure of the flowing fluids can be obtained by equations that are represented as follow[41, 42]:

Table 3.Partial pressure of H2 and O2at the three-phase boundary[42].

Equation	No.
$P_{H_2,TBP} = P_{H_2,f} - \frac{RT_{cell} \tau_{anode}}{2FD_{eff,anode}} j$	7
$P_{O_2,TBP} = p - (p - p_{O_2,a}) \exp(\frac{RT_{cell} \tau_{anode}}{4FD_{eff,anode}} j)$	8

The designing functional factors of SOFCs are listed in table 4. The temperature of the air that

enters into the cathode is acquired by primary calculations. One of the main focused parameters in the SOFC analysis model is the temperature gradient that is less than 100 K in our work.

Table 4. SOFC operational factors [43, 44].

Parameters	Symbol	Value
Ratio of oxygen-fuel	$R_{cell}$	2.7
Fuel consumption	$\eta_f$	0.8
Temperature of the cathode air inlet	$T_a$	903 (K)
Parameter of total pressure recovery	$\xi_{cell}$	3%

Articles can be up to 10 pages in length. The main text (not including abstract, Methods, References and figure legends) is limited to 5,000 words. The

maximum title length is 15 words. The main text of an Article should begin with an introduction (without heading) of referenced text that expands on the background of the work (some overlap with the abstract is acceptable), followed by sections headed Results, Discussion (if appropriate) and Methods (if appropriate). The Results and Methods sections may be divided by topical subheadings; the Discussion should be succinct and may not contain subheadings. Figure legends are limited to 350 words each. References are limited to 70. Footnotes are not used.

If you choose not to use this document as a template, prepare your technical work in single-spaced, double-column format. Set bottom margins to 25 millimeters (0.98 inch) and top, left and right margins to about 20 millimeters (0.79 inch). Margin of First page is different from other pages. For first page set top margin to 30 millimeters (1.18inch), and bottom, left and right margins are similar to other pages. Do not violate margins (i.e., text, tables, figures, and equations may not extend into the margins). The column width is 78 millimeters (3.07 inches). The space between the two columns is 13 millimeters (0.51 inch).

### 3.3. Jet engine model

The thermodynamic analysis equations of the intake, compressor, nozzle, and combustor in both suggested cycles are considered as follow:

**Table 5. Thermodynamics equations of the components [31, 45].**

Components	Equation	No.
Intake	$= T_{in} \{1 + (\frac{\gamma-1}{2}) M_{\infty}^2\}$	9
	$P_{out} = P_{in} \{1 + \eta_{inta} \left[ \left( \frac{T_{out}}{T_{in}} \right) - 1 \right] \}^{\gamma/(\gamma-1)}$	10
	$\eta_{inta} = 1 - 0.075(M_{\infty} - 1)^{1.35}$	11
Compressor	$T_{out} = \left\{ 1 + \left( \frac{1}{\eta_{comp}} \right) \left[ \left( \pi \right)^{\frac{\gamma-1}{\gamma}} - 1 \right] \right\} T_{in}$	12
	$P_{out} = P_{in} \pi_{comp}$	13
	$W_{comp} = h_{comp,out} - h_{comp,in}$	14
	$\eta_{comp} = 0.91 - \frac{\pi_{comp} - 1}{300}$	15
Nozzle	$u_e = \sqrt{2\eta_{nozz} c_p T_{in} \left( 1 - \left( \frac{p_a}{p_{in}} \right)^{(\gamma-1)/\gamma} \right)}$	16
	$p_{out} = p_a$	17
Combustor	$H_{comb,out} = H_{SOFC,out} H_{fb,in}$	18

The total pressure recovery coefficient of the intake is considered under the experimental result assumptions of NASA. The compressor adiabatic efficiency is calculated employing the Korakianitis and Wilson equations [46]. For the standard operating condition of jet engines, the efficiency and total pressure recovery multiplier of the combustor and adiabatic efficiency of the nozzle applied in both cycles are listed in table 6.

**Table 6. Efficiency coefficients of combustor and nozzle [32, 47].**

Component	Symbol	Value
Efficiency of combustor	$\eta_{comb}$	0.98
Multiplier of combustor total pressure recovery	$\xi_{comb}$	0.99
Efficiency of nozzle	$\eta_{nozz}$	0.9

### 3.5. Heat exchanger and blower model

The analysis method of the heat exchanger generally depends on the equations of energy conservation and the blower working temperature that is the mixed gas temperature. The blower outlet condition can be calculated by the following equations [26, 48]:

$$T_{out} = \left\{ 1 + \left( \frac{1}{\eta_{blow}} \right) \left[ \pi_{blow}^{\frac{\gamma-1}{\gamma}} - 1 \right] \right\} T_{in} \tag{19}$$

$$P_{out} = P_{in} \pi_{blow} \tag{20}$$

$$W_{blow} = h_{blow,out} - h_{blow,in} \tag{21}$$

The working conditions of the heat exchanger and blower are shown in table 7.

**Table 7. Working factors of the blower and heat exchanger[48].**

Element	Symbol	Value
Efficiency of heat exchanger	$\eta_{ex}$	0.98
Gas section parameter of pressure recovery	$\eta_{ex,g}$	0.99
Adiabatic efficiency of blower	$\eta_{blow}$	0.7
Pressure ratio of blower	$\pi_{blow}$	1.1
Air section parameter of pressure recovery	$\eta_{ex,a}$	0.98

### 3.6. Performance factors

For the suggested propulsion system in this work that SOFCs has the main role in converting energy, table 8 indicates several factors affecting the performance of the fuel cells. The endurance can be estimated by specific impulse, and the thrust-weight ratio is quantified by the specific thrust. Moreover, the propulsion efficiency and overall efficiency develop a relationship between the engine and the environment [49].

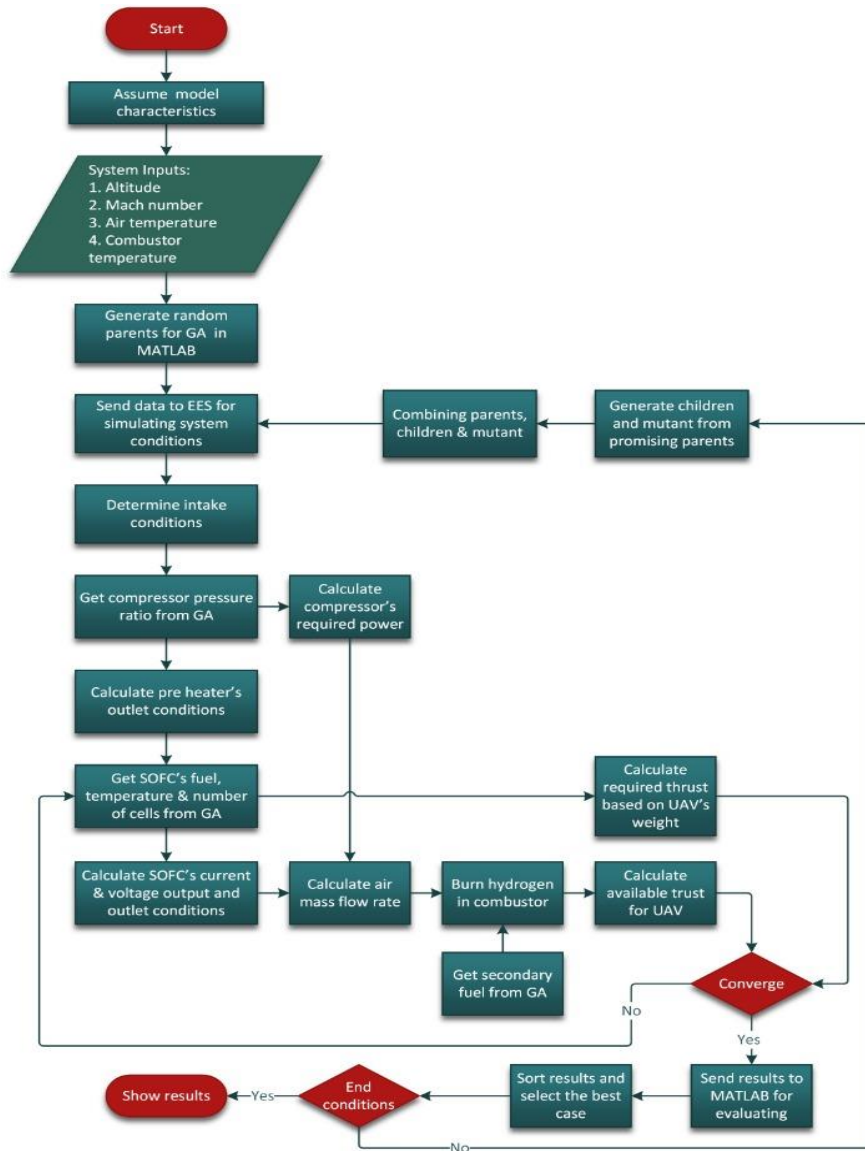
**Table 8. Efficiency equations of the system [50, 51].**

Component	Equations	No.
Thermal efficiency	$\eta_{ther} = (KE_{gain}) / (\dot{m}_f \times Q_r) \times 100$	22
Propulsion efficiency	$\eta_{prop} = \frac{2}{1 + u_e/u} \times 100$	23
Overall efficiency	$\eta_{over} = \eta_{ther} \eta_{prop} \times 100$	24

**3.6. Solution method**

The analysis of SOFC simulated operation begins with the input data such as the intake air temperature, compressor pressure ratio, fuel mass flow rate, flight Mach number, and altitude. The first step in simulating the proposed propulsion system is to import the key design parameters from the genetic algorithm in MATLAB that includes the compressor pressure ratio. Next, based on the intake air conditions, the properties of the outlet stream of the compressor can be calculated, which will be used to simulate the

voltage and current of SOFCs based on the other imported key design parameters such as the fuel mass flow rate, number of cells, and stack temperature. Since the power generated by SOFCs will operate the electric motor for the compressor, the air mass flow rate can be calculated from the compressor pressure ratio and power generated by SOFCs. Then the unused fuel in SOFCs will be burnt in the afterburner in order to generate the heat required for the generation of thrust in the nozzle. Additional fuel might be added if a higher thrust is needed based on the required thrust to weight ratio. Next, the results of the simulation will be sent to GA in MATLAB in order to sort the best answers and repeat the process to achieve the best solution that satisfies the optimization goals [52, 53]. Figure 2 demonstrates the overall procedures for simulation and optimization of the proposed system.



(a)

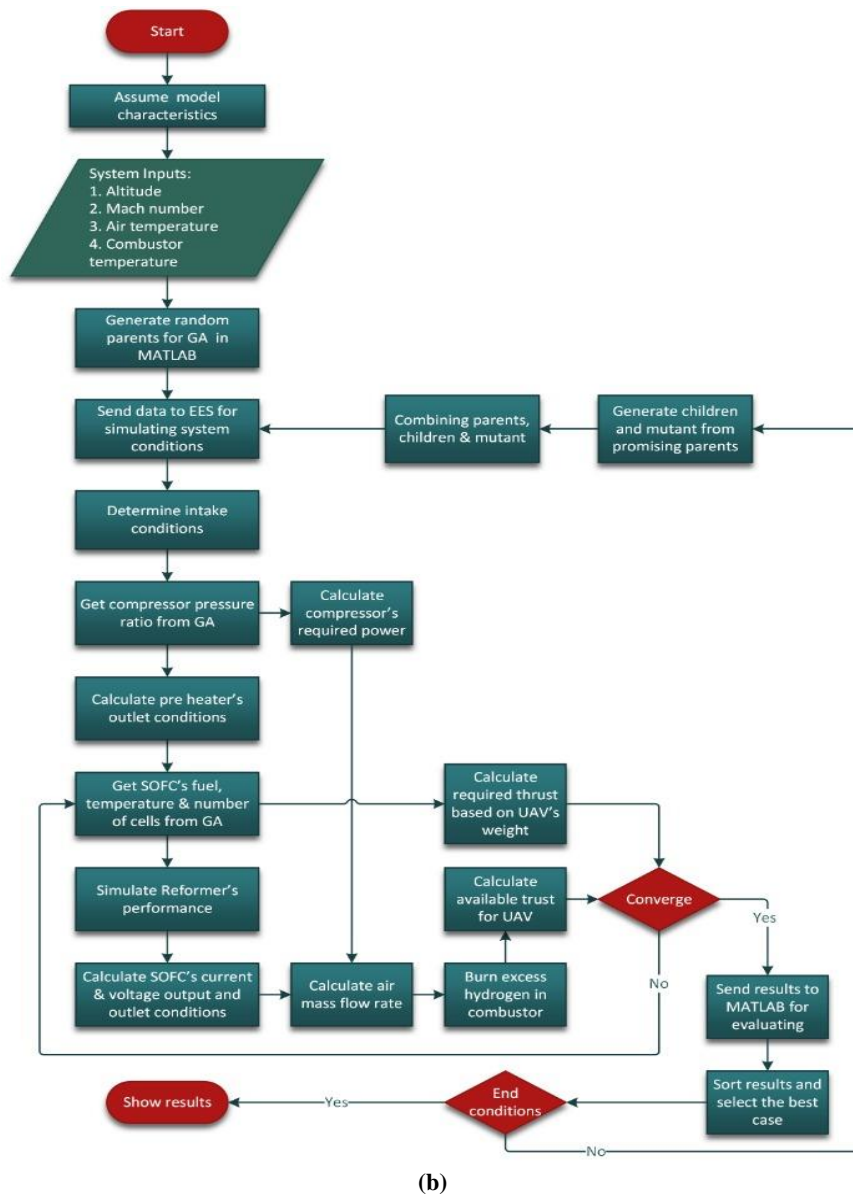


Figure 2. A flowchart to investigate performance of the suggested propulsion system (a) hydrogen-fueled (b) methane-fueled.

### 3.8. Optimization

The optimization algorithms are considered one of the promising methods for solving the complex engineering problems when simple calculations are not effective to portrait the system reaction to the changes in the operating conditions of the system components. Since in the proposed propulsion system many of the key design parameters may conflict with each other, using the heuristic numerical algorithms such as the genetic algorithm (GA) can be extremely beneficial. Two goals for optimization of the proposed propulsion system are defined: (1) maximizing the thrust (2) minimizing the fuel consumption rate. These are the main goals of the aviation industry that can be interpreted as the maximum efficiency. In order to design the proposed propulsion system to satisfy the goals, a multi-objective optimization was employed to maximize the thrust, while

minimizing the fuel consumption rate (i.e. maximizing the flight duration). For this purpose, a new optimization target consists of two separate dimensionless parameters as thrust, and the fuel consumption rate is defined (as shown in Eq.25). By changing the weight ( $\alpha$ ) for each one of these dimensionless parameters, a working curve will be generated that is known as the Pareto frontier. Finally, the TOPSIS decision-making method was used in order to select the best answer with an acceptable trade-off between thrust and fuel consumption. In the TOPSIS approach, the decisions are possible if there are positive and negative criteria (even together in one issue). The positive criteria are the ones that have a profit aspect such as the product quality, and the negative criteria are the ones that have a loss aspect such as hard work. In order to determine the best option, a significant number of criteria

can be considered, while the AHP method or the ANP method has practical and inherent limitations in this area. This method is simple and has a good speed, and is well-responsive for many options and criteria. In the TOPSIS method, the qualitative criteria can be easily quantified, and the decisions can be made despite the qualitative and quantitative criteria. The output of the system is quantitative, and in addition to determining the superior option, the ranking of the other options is expressed numerically. This numerical value is the relative proximity that expresses the strong foundation of this method [54, 55]. The TOPSIS method has good mathematical foundations. This method deals with distances. TOPSIS selects the option with the farthest distance from the worst option and the shortest distance from the best option as the optimal option, and for this reason, and its mathematical basis, is superior to the other methods. The TOPSIS method has another advantage over some other methods, and is a compensatory method, i.e., the weight of all options and criteria is involved in the decision, and no weight is ignored in this method [53, 56].

$$Obj. = \alpha \frac{Thrust_{max}}{Thrust} + (1 - \alpha) \frac{Fuel\ mass\ flow\ rate}{Fuel\ mass\ flow\ rate_{min}} \quad (25)$$

**Table9.**List of parameters for system optimization.

Key design and optimization parameters	Range or value
SOFC fuel mass flow rate (kg/s)	$0.001 < \dot{m}_{fuel} < 0.015$
Secondary fuel mass flow rate (kg/s)	$0 < \dot{m}_{fuel,2} < 0.0005$
Compressor pressure ratio	$5 < R < 25$
Anode recirculation ratio (for methane-fuel only)	$0.4 < \alpha < 0.8$
SOFC's temperature (K)	$900 < T_{stack} < 1300$
SOFC's cell number	$1500 < N_c < 6000$
Population size	20
Max number of generations	250
Probability of off-spring	0.8
Probability of mutation	0.3
Mutation rate	0.02
Exploration	0.05
Number of cross-over points	1
Selection method	Roulette wheel
Selection pressure	5

#### 4. Validation

The results of the simulation of the proposed propulsion system were compared with the similar results reported by the other authors. For this purpose, the working conditions of the proposed system by Zhixing et al. [44] were used for

simulating the system proposed in this work. table 10-1 to 10-3 compares the simulated temperature and pressure of the current work for each point, and also the efficiency and thrust with the data reported by Zhixing et al. [32]. As seen, a desirable agreement can be noticed. Also a similar comparison was conducted for the methane-fuel system in table 10-2.

**Table 10-1.** Simulated temperature and pressure for each point in the hydrogen-fueled system and data reported by Zhixing et al.[32].

Stage	This work		Zhixing[44]et al.		Error (%)	
	T(K)	P(Bar)	T(k)	P(bar)	T(K)	P(bar)
1	288	1.0	288	1	0.00	0.00
2	673.1	15.0	675	15	0.28	0.03
3	873	15.0	843	15	0.00	0.03
4	300	15.0	300	15	0.00	0.03
5	873	15.0	873	15	0.00	0.03
6	1016	14.3	1046	14	2.87	1.82
7	1016	14.3	1046	14	2.87	1.82
8	1016	14.3	1046	14	2.87	1.82
10	1147	14.3	1167	14	1.71	1.82
11	1053	14.3	993	14	6.04	1.82
12	923	14.3	946	14	2.41	1.82
13	490	14.3	516	1	4.98	1.82

**Table 10-2.** Simulated temperature and pressure for each point in the methane-fueled system and data reported by Zhixing et al.[32].

Stage	This work		Zhixing[44]et al.		Error (%)	
	T(K)	P(Bar)	T(k)	P(bar)	T(K)	P(bar)
1	288	1.0	288	1	0.00	0.00
2	673.1	15.0	675	15	0.28	0.01
3	300	14.3	300	15	0.00	4.99
4	958.9	14.3	1008	14	4.87	1.79
5	908.4	14.3	896	14	1.38	1.79
6	918.9	15.0	912	16	0.76	6.24
7	673.1	15.0	675	15	0.28	0.01
8	900	15.0	907	15	0.77	0.01
9	925	14.3	874	15	5.84	4.99
10	673.1	15.0	675	15	0.28	0.01
11	873	15.0	873	15	0.00	0.01
12	958.9	14.3	1008	14	4.87	1.79
13	958.9	14.3	1008	14	4.87	1.79
14	958.9	15.0	1008	14	4.87	7.15
15	958.9	14.6	1008	14	4.87	4.47
16	1033	14.6	1078	14	4.17	4.47
17	850.6	14.6	898	14	5.28	4.47
18	466.8	1	487	1	4.15	0.00

**Table 10-3. Efficiency, cell voltage, and thrust for the proposed systems and data reported by Zhixing et al.[32].**

	Hydrogen			Methane		
	This work	Zhixing et al. [44]	Error (%)	This work	Zhixing et al. [44]	Error (%)
Efficiency (%)	63.2	61.5	2.76	65.28	67.7	3.57
Cell voltage (V)	0.869	0.845	2.84	0.865	0.845	2.37
Thrust (N)	948.1	1000	5.19	903.2	970	6.89

Additionally, table 9-3 compares the efficiency, cell voltage, and thrust for proposed systems with the results reported by Zhixing et al.[32].

**5. Results and Discussion**

In the case of comparing the performance of two hybrid turbine-less configurations of the supersonic propulsion system in this work, a numerical simulation of the operating condition was performed. Firstly, the weight of the UAV with regard to the SOFC size was estimated, and due to this variable, the amount of the required thrust for the vehicle could be calculated. Furthermore, the performance of the two systems was compared by different parameters such as the flight altitude, fuel mass flow rate, compressor pressure ratio, and SOFC temperature. Finally, the optimum amounts of the thrust and fuel consumption as the key parameters of the system performance were calculated by the TOPSIS method.

As mentioned earlier, by changing the weight (percentage of the impact of each goal) for the dimensionless thrust and fuel mass flow rate in the multi-objective optimization target, the optimum working condition will change. These working points create a working curve in which each point on this curve is related to a specific weight, as shown in Eq.25. This working curve that is known for the Pareto frontier is demonstrated in figure 3. If the weight is set to 1, the optimization will only maximize the thrust with no restriction on the fuel mass flow rate (A); subsequently, if the weight is

set to 0, the optimization will only minimize the fuel mass flow rate with no restriction on the thrust (B).

In order to obtain the best working point for these proposed systems, the TOPSIS decision-making method was used. This method designates two points as the imaginary best and worst points, and selects the optimum answer in a way that the selected point has the minimum and maximum distances to the imaginary best and worst points, respectively. The optimum working conditions for both proposed propulsion systems are illustrated in table 11. Also the stream properties of the hydrogen- and methane-fueled propulsion systems are shown in tables 12 and 13, respectively.

**Table 11. Optimized working conditions for the proposed propulsion systems.**

	Hydrogen-fueled	Methane-fueled
Compressor pressure ratio	11.797	8.6502
SOFC's fuel mass flow rate (g/s)	2.3808	6.507
Combustor fuel mass flow rate (g/s)	0.0585	-
Anode recirculation ratio	-	0.8
Stack temperature	1064	1020.7693
SOFC's cell number	3332	5045.3183
Air (kg/s)	0.34032	0.593
Thrust(N)	182.8518	219.4525
Efficiency (%)	48.755	67.91
Fuel consumption(kg/s)	0.0024	0.0065

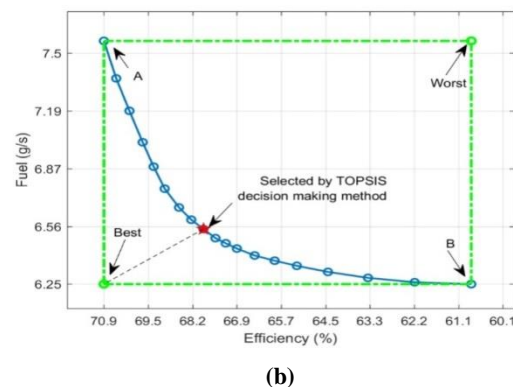
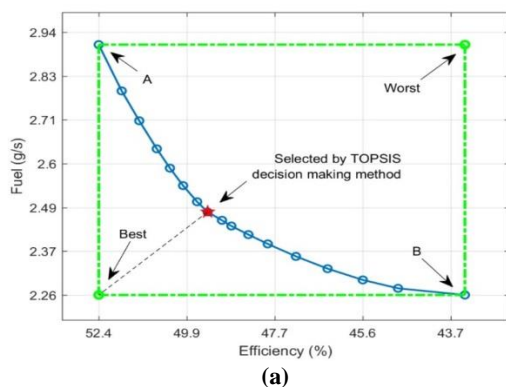


**Figure 3. Optimized points for fuel consumption and generated thrust of the two proposed systems (a) hydrogen-fueled (b) methane-fueled.**

In order to study the system responses to the changes in the key design parameters and different flight altitudes, a sensitivity analysis was performed to find out the changes in the efficiency, SOFC's power generation, fuel and air mass flow rate, and thrust based on which a parameter is investigated. For this purpose, all the

key design parameters were fixed at the optimum operation condition obtained from the GA results and TOPSIS methods' decision and vary a single parameter in the range that the system can be operated at. In the following, each one of these key parameters is discussed.

**Table 12. Stream properties of hydrogen-fueled propulsion system.**

Stage	T (K)	P (bar)	m (kg/s)	h (kJ/kg)	H <sub>2</sub> O (%)	H <sub>2</sub> (%)	N <sub>2</sub> (%)	O <sub>2</sub> (%)
0	223	0.26	0.3403	6465	0	0	79	21
1	367.9	1.38	0.3403	10684	0	0	79	21
2	767.2	16.32	0.3403	22778	0	0	79	21
3	954.9	16.32	0.3403	28825	0	0	79	21
4	300	100.96	0.002381	8076	0	100	0	0
5	954.9	16.32	0.002381	27284	0	100	0	0
6	1064	15.50	0.3262	30946	0	0	82.08	17.92
7	1064	15.50	0.01655	63467	75	25	0	0
8	1064	15.50	0.3427	34010	7.066	2.355	74.35	16.23
9	300	100.96	0.0000585	8076	0	100	0	0
10	1205	15.50	0.3428	40035	9.483	0.2611	75.05	15.21
11	1153	15.50	0.3428	38208	9.483	0.2611	75.05	15.21
12	985.3	15.50	0.3428	32464	9.483	0.2611	75.05	15.21
13	288.4	0.26	0.3428	8364	9.483	0.2611	75.05	15.21

**Table 13. Stream properties of methane-fueled propulsion system.**

Stage	T (K)	P (bar)	m (kg/s)	h (kJ/kg)	CH <sub>4</sub> (%)	CO <sub>2</sub> (%)	CO (%)	H <sub>2</sub> O (%)	H <sub>2</sub> (%)	N <sub>2</sub> (%)	O <sub>2</sub> (%)
0	223.3	0.26	0.5901	6472	0	0	0	0	0	79	21
1	368.3	1.41	0.5901	10696	0	0	0	0	0	79	21
2	723.1	12.20	0.5901	21391	0	0	0	0	0	79	21
3	300	11.59	0.006546	-117	100	0	0	0	0	0	0
4	1021	11.59	0.186	61873	0.00316	18.65	1.055	72.92	4.861	1.985	0.5277
5	996.3	11.59	0.1926	59765	4.699	17.78	1.006	69.49	4.633	1.892	0.5029
6	1008	12.20	0.1926	60252	4.699	17.78	1.006	69.49	4.633	1.892	0.5029
7	723.1	12.20	0.001501	21391	0	0	0	0	0	79	21
8	1005	12.20	0.1941	59951	4.671	17.67	0.9998	69.08	4.605	2.351	0.6249
9	1070	11.59	0.1941	56196	0.00342	20.2	1.143	54.87	21.06	2.15	0.5715
10	723.1	12.20	0.5886	21391	0	0	0	0	0	79	21
11	995	11.59	0.5886	30143	0	0	0	0	0	79	21
12	1021	11.59	0.2325	61873	0.00316	18.65	1.055	72.92	4.861	1.985	0.5277
13	1021	11.59	0.0465	61873	0.00316	18.65	1.055	72.92	4.861	1.985	0.5277
14	1021	11.59	0.5644	29495	0	0	0	0	0	82.03	17.97
15	1021	11.59	0.6109	32581	0.0003	1.778	0.1006	6.951	0.4634	74.4	16.3
16	1057	11.59	0.6109	34055	6.03E-06	1.882	0.00202	7.426	0.00929	74.61	16.07
17	812.3	11.59	0.6109	25810	6.03E-06	1.882	0.00202	7.426	0.00929	74.61	16.07
18	254.4	0.26	0.6109	7376	6.03E-06	1.882	0.00202	7.426	0.00929	74.61	16.07

### 5.1. Flight altitude

As illustrated in figure 4, for the methane-fueled system, the efficiency and generated power of the propulsion system increases as the flight altitude rises; this is due to the existence of the reformer and recirculation of the unused fuel that affects the fuel utilization inside the SOFC, thus resulting in a higher thermal efficiency. This phenomenon can help the UAV to be capable of operating at high-altitude missions. On the other hand, the hydrogen-fueled system shows more potential for low-altitude missions since by increasing the

altitude, the efficiency drops; contradicting to the hydrogen-fueled system, the methane-fueled system's efficiency increases at higher altitudes, and ultimately becomes constant, which is ideal for long-term flights in high altitudes. In both systems, it was found that the fuel consumption rate dropped as altitude increased due to lower air temperature, which reduced the compressor power, and decreasing in the air resistance force that requires a lower thrust. However, the air mass flow rate increases at higher altitudes.

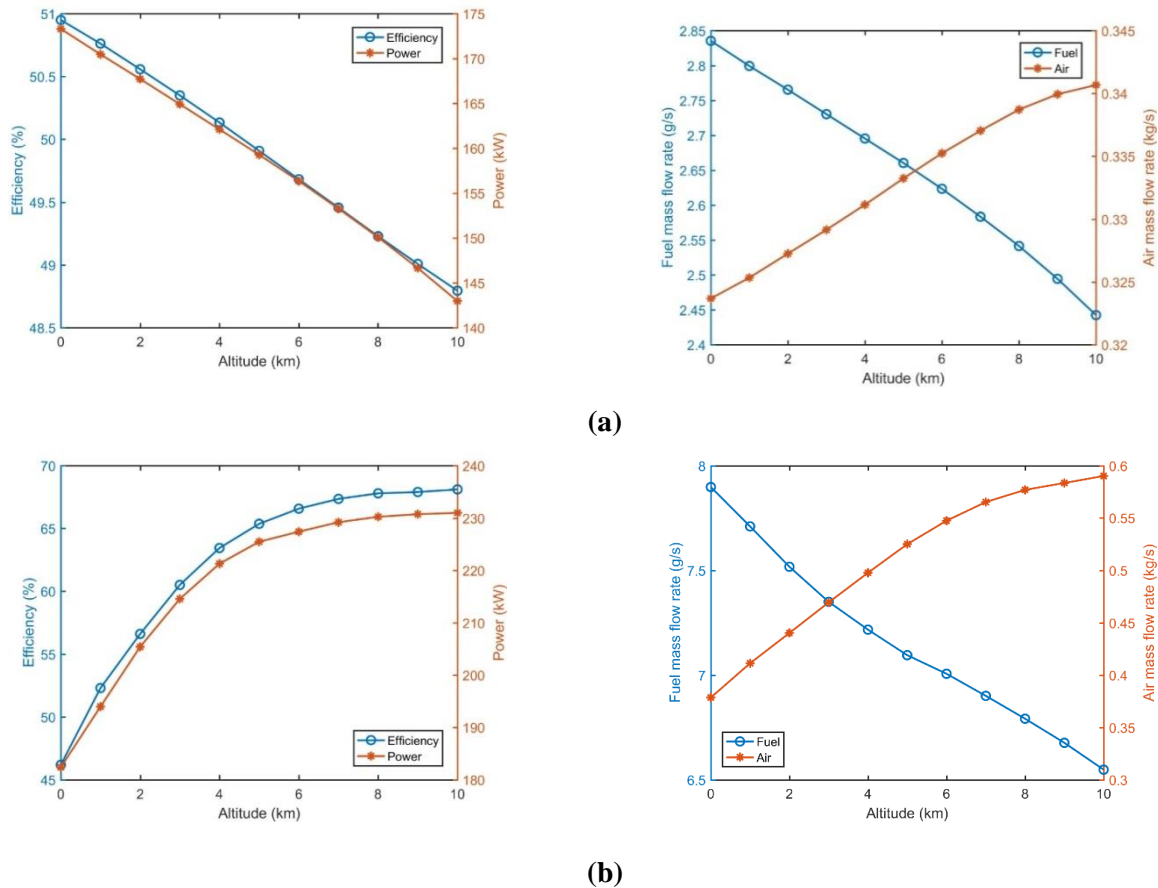


Figure 4. System responses to changes of flight altitude (a) hydrogen (b) methane.

### 5.2. SOFC fuel mass flow rate

The amount of thrust that is generated by an engine is important. However, the amount of fuel used to generate that thrust sometimes has a more significant importance since the UAV has to lift and carry the additional fuel with the main necessary instruments for the long-endurance missions. As depicted in figure 5, increasing the fuel mass flow rate of the SOFC by when other key parameters are in optimum condition will generate extra electrical power and higher thrust for the UAV; however, this higher fuel rate will decrease the efficiency, thus resulting in a lower

flight endurance. The results obtained state that the hydrogen-fueled SOFC system is a suitable candidate for a fuel mass flow rate range of 1 to 5 g/s and a power range of 60-240 kW. However, the methane-fueled system exhibits a power range of 180-320 kW and a fuel mass flow rate of 5-15 g/s. Also note that the fuel mass flow rate cannot be lower than 2.4 g/s and 6.56 g/s for the hydrogen-fueled and methane-fueled systems, respectively since the generated thrust becomes insufficient to maintain the current speed and altitude of the UAV.

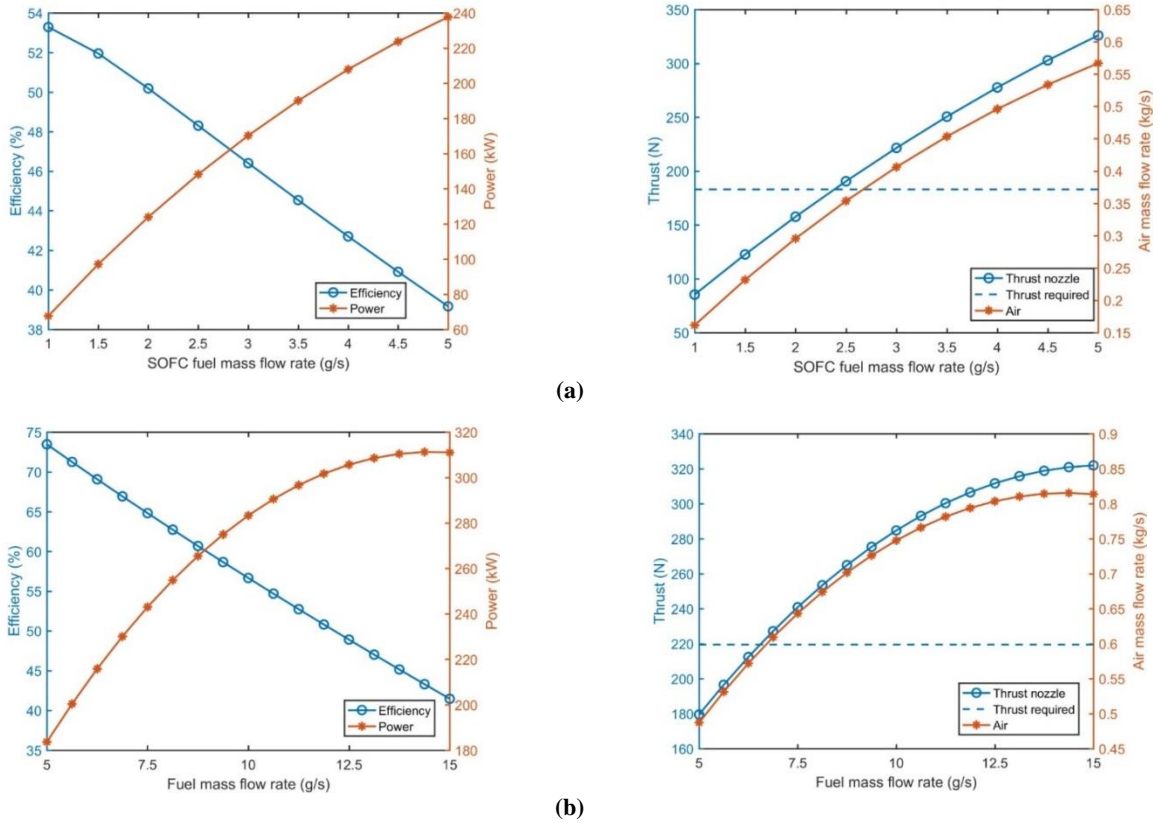


Figure 5. System responses to changes of SOFC's fuel mass flow rate (a) hydrogen (b) methane.

### 5.3. Compressor pressure ration

The pressure ratio is considered a major factor in the operation of UAVs with hybrid turbine-less SOFC jet engines. Figure 6 demonstrates the system responses to the changes in the compressor pressure ratio in Mach 1.8. As seen, the efficiency of the power generated by the SOFC propulsion system and thrust raise with the increase in the compressor pressure ratio. This increase in the thrust for the propulsion power is due to the

increment of the nozzle pressure ratio. Furthermore, by increasing the pressure ratio of the compressor and constancy of the generated electric power of fuel cell, the efficiency of fuel cell lightly increases. By correlating figures 6(a) and 6(b), it can be concluded that the hydrogen-fueled system generates a less power and has a lower efficiency, and this can be due to the higher utilization of fuel with the help of recirculation of the unused fuel.

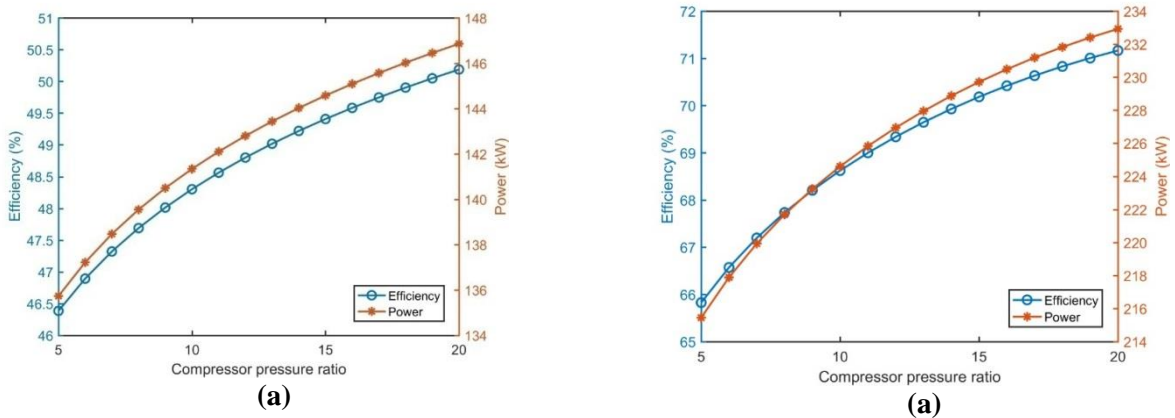


Figure 6. Efficiency and power changes as a function of compressor pressure ratio (a) hydrogen (b) methane.

### 5.4. Stack Temperature

As it can be seen in figure 7, the stack temperature plays a major role in the efficiency of the SOFC power generation that also effectively changes the thrust of the engine. As indicated in the figures, for both hydrogen- and methane-fueled systems, the maximum efficiency happens around the stack temperature of 1025 K but this is not in agreement with where the maximum thrust happens around 1075 K. It can be concluded that whether the optimization target is set to maximum efficiency or thrust, the operating conditions may differ, which is the main reason why the cruise speed is different and lower than the maximum speed in

the airplanes. Additionally, since one of the objectives of the optimization is to minimize the fuel consumption, as seen in the figure, at the optimum working conditions, the available thrust from the engine and the required thrust for maintaining the current flight profile is equivalent. Thus even the slightest changes in the stack temperature may result in an inconsistency in the flight profile, which is not demanding. From this fact, it can be suggested that the future researchers that use a similar pattern for the optimization or design of the UAV engines use a safety factor in order to ensure that this inconsistency never happens for at least small changes.

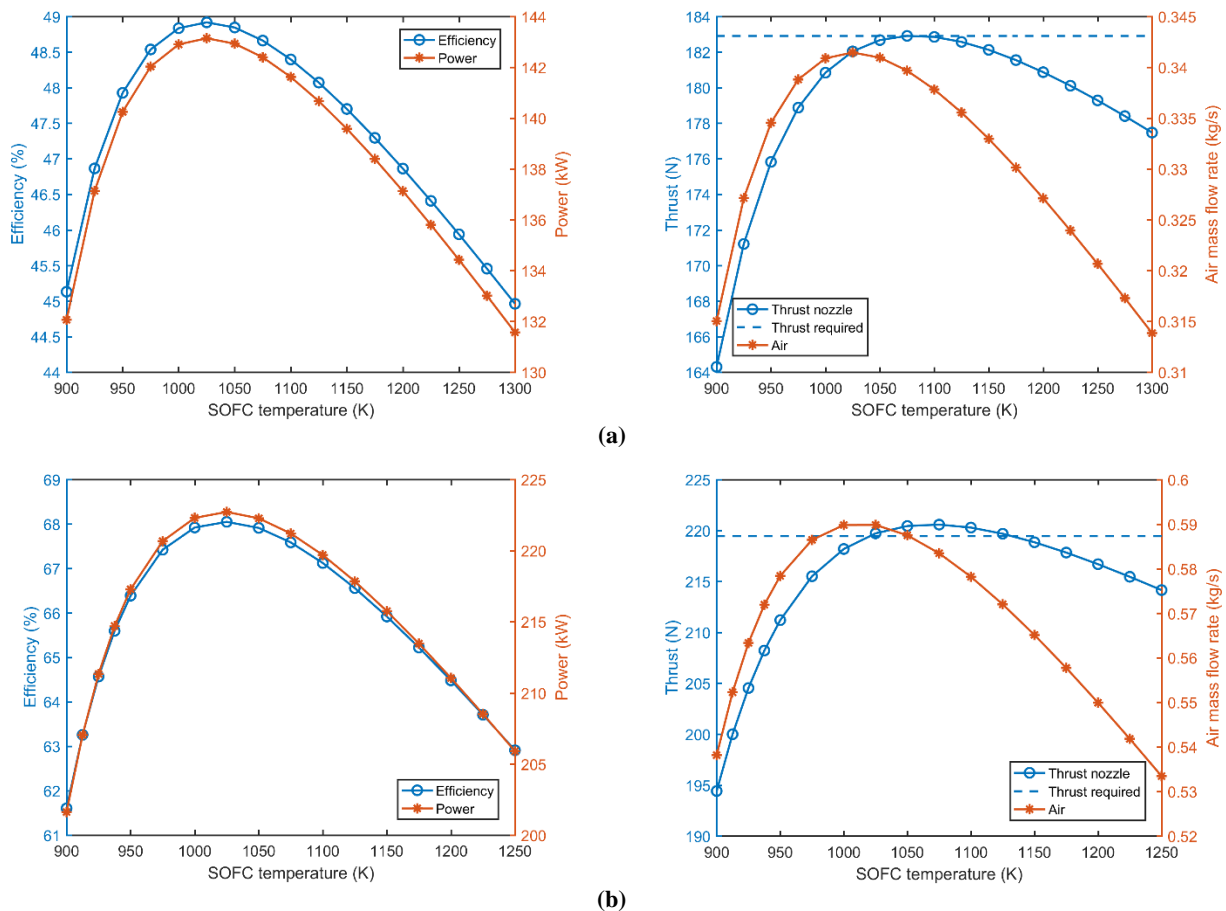


Figure 7. System responses to changes of stack temperature (a) hydrogen (b) methane.

### 5.5. Cell numbers

Although the number of cells in the SOFC is constant and will not change during the flight and midair, however, different numbers of cells will result in different voltages and currents, which varies the generated power of the SOFC as increasing the cell numbers will increase the efficiency and thrust. Moreover, changing the number of cells varies the weight of the UAV and changes the required thrust and power. As seen in

figure 8, increasing the cell numbers will result in a higher power generation and thrust but if the number of cells increases without changing the other design parameters, there is a lower and upper limit for the cell number. As indicated in figure 8, for the hydrogen-fuel system, the range of available cell numbers is from 1750 to 3250, and for the methane-fuel system, the mentioned range is from 3500 to 5250.

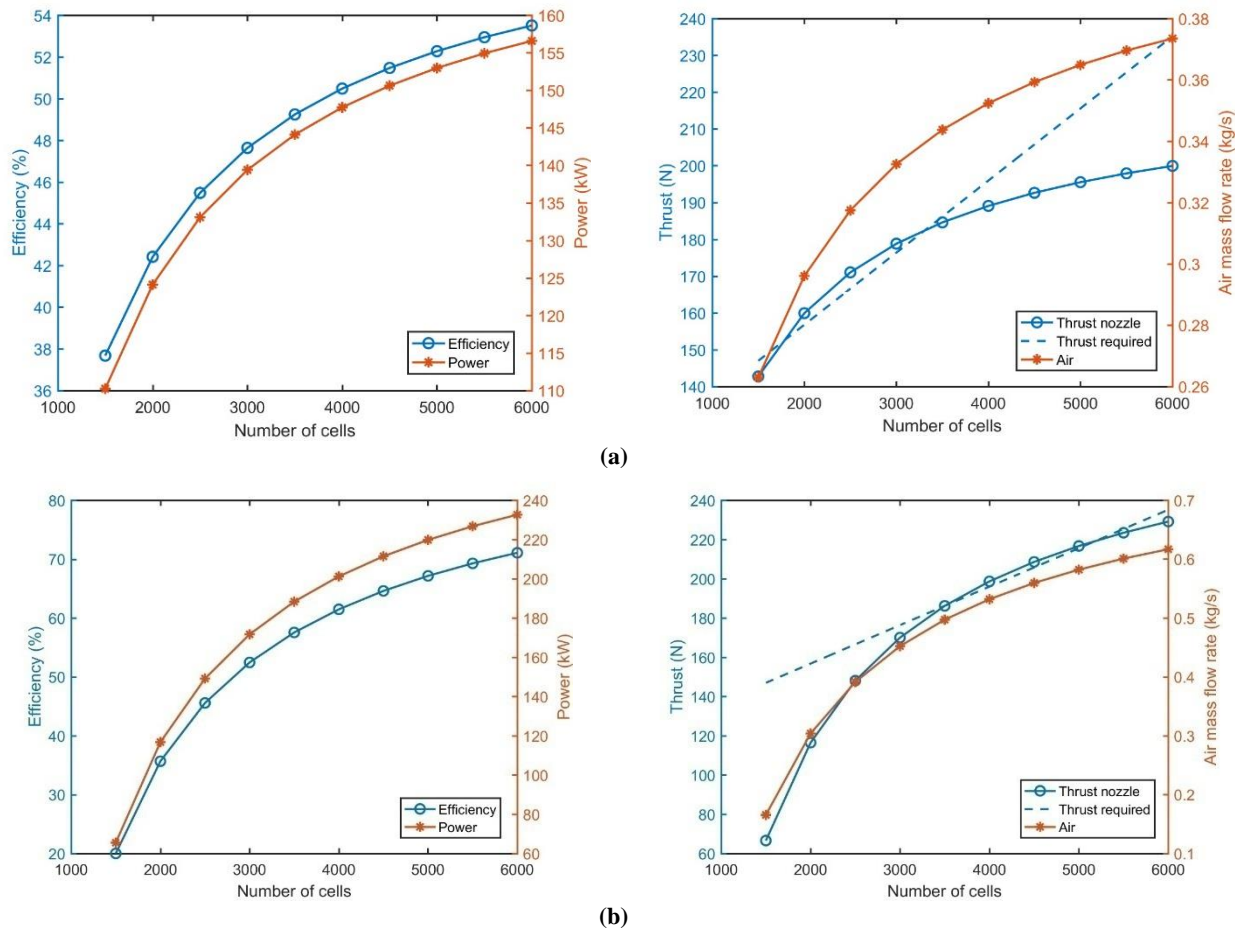


Figure 8. System responses to changes in number of cells (a) hydrogen (b) methane.

### 6. Conclusions

In the case of comparing the performance of two hybrid turbine-less configurations of the supersonic power unit in this work with hydrogen and methane as different types of fuel, a numerical simulation of the operating condition was performed. The thermodynamic parameters of both systems were studied under the condition of supersonic flight mode with the Mach number 1.8. Finally, the generated thrust and consumed fuel, as the key parameters of the flight, were optimized by the genetic algorithm and the TOPSIS method. The main results of this work are as follow:

1. The efficiency and generated power of the propulsion system by increasing the flight altitude increase in the case of the methane-fuel system.
2. Low temperature at high-altitude flight levels in the case of a fixed Mach number, and the compressor pressure ratio leads to an increment in the intake air mass flow rate of the system.
3. The increasing fuel rate of the SOFC power unit helps the process of generating extra

power and thrust for UAVs. However, the high fuel mass flow rate drops the fuel cell efficiency, which generally makes the flight endurance low.

4. By increasing the pressure ratio of the compressor and constancy of the generated electric power of the fuel cell, the efficiency of the fuel cell lightly increases. The methane-fueled system generates a higher power and efficiency due to the recirculation of the unused fuel.
5. By increasing the cell numbers, the efficiency of the system rises due to improvement in the generated power and thrust. The simulation results state that the thrust and consumed air of the hydrogen-fueled power unit are less than the methane-fueled.
6. The maximum efficiency for both the hydrogen- and methane-fueled systems is available with the stack temperature of 1025 K. However, the maximum thrust for these systems is at the stack temperature of 1075 K.
7. For the current work, the thrust and fuel consumption were the parameters that were

optimized by the multi-objective optimization method for both systems. The efficiency and fuel consumption for the hydrogen-fueled system are 48.7% and 0.0024 g/s, and for the methane-fueled system, are 67.9% and 0.0066 g/s.

The future studies could focus on the SOFCs with higher power densities. In addition, the size of the various configurations could be calculated in the future research works. The experimental implementation of a propulsion system for UAVs could also be considered.

## 7. References

- [1] Marefati, M., M. Mehrpooya, and S.A. Mousavi, Introducing an integrated SOFC, linear Fresnel solar field, Stirling engine and steam turbine combined cooling, heating and power process. *International Journal of Hydrogen Energy*, 2019.
- [2] Peng, M.Y.-P. et al., Energy and exergy analysis of a new combined concentrating solar collector, solid oxide fuel cell, and steam turbine CCHP system. *Sustainable Energy Technologies and Assessments*, 2020. 39: p. 100713.
- [3] Buonomano, A. et al., Hybrid solid oxide fuel cells–gas turbine systems for combined heat and power: A review. *Applied Energy*, 2015. 156: p. 32-85.
- [4] Sadeghi, H. et al., Numerical Investigation of Gas Channel Geometry of Proton Exchange Membrane Fuel Cell. *Renewable Energy Research and Applications*, 2020. 1(1): p. 93-114.
- [5] Rostami, M. and A.h. Farajollahi, Aerodynamic performance of mutual interaction tandem propellers with ducted UAV. *Aerospace Science and Technology*, 2021. 108: p. 106399.
- [6] Marchant, W. and S. Tosunoglu. Rethinking wildfire suppression with swarm robotics. in *Proceedings of the 29th Florida Conference on Recent Advances in Robotics, FCRAR*. 2016.
- [7] Rechberger, J. et al., Demonstration of the first European SOFC APU on a heavy duty truck. *Transportation Research Procedia*, 2016. 14: p. 3676-3685.
- [8] Kaya, N. et al., Parametric study of exergetic sustainability performances of a high altitude long endurance unmanned air vehicle using hydrogen fuel. *International Journal of Hydrogen Energy*, 2016. 41(19): p. 8323-8336.
- [9] Cirigliano, D. et al., Diesel, spark-ignition, and turboprop engines for long-duration unmanned air flights. *Journal of Propulsion and Power*, 2018. 34(4): p. 878-892.
- [10] Beigzadeh, M., F. Pourfayaz, and S.M. Pourkiaei, Modeling Heat and Power Generation for Green Buildings based on Solid Oxide Fuel Cells and Renewable Fuels (Biogas). *Renewable Energy Research and Applications*, 2020. 1(1): p. 55-63.
- [11] Rostami, M., M. Dehghan Manshadi, and E. Afshari, Performance evaluation of two proton exchange membrane and alkaline fuel cells for use in UAVs by investigating the effect of operating altitude. *International Journal of Energy Research*, 2021.
- [12] Eisavi, B. et al., Thermo-environmental and economic comparison of three different arrangements of solid oxide fuel cell-gas turbine (SOFC-GT) hybrid systems. *Energy Conversion and Management*, 2018. 168: p. 343-356.
- [13] Alirahmi, S.M., M. Rostami, and A.H. Farajollahi, Multi-criteria design optimization and thermodynamic analysis of a novel multi-generation energy system for hydrogen, cooling, heating, power, and freshwater. *International Journal of Hydrogen Energy*, 2020.
- [14] Tucker, M.C., Development of High Power Density Metal-Supported Solid Oxide Fuel Cells. *Energy Technology*, 2017. 5(12): p. 2175-2181.
- [15] Azizi, M.A. and J. Brouwer, Progress in solid oxide fuel cell-gas turbine hybrid power systems: System design and analysis, transient operation, controls and optimization. *Applied energy*, 2018. 215: p. 237-289.
- [16] Alayi, R., et al., Optimization, Sensitivity Analysis, and Techno-Economic Evaluation of a Multi-Source System for an Urban Community: a Case Study. *Renewable Energy Research and Applications*, 2021: p. -.
- [17] Beiranvand, A. et al., Energy, Exergy, and Economic Analyses and Optimization of Solar Organic Rankine Cycle with Multi-objective Particle Swarm Algorithm. *Renewable Energy Research and Applications*, 2021. 2(1): p. 9-23.
- [18] Himansu, A. et al., Hybrid solid oxide fuel cell/gas turbine system design for high altitude long endurance aerospace missions. 2006.
- [19] Aguiar, P., D. Brett, and N. Brandon, Solid oxide fuel cell/gas turbine hybrid system analysis for high-altitude long-endurance unmanned aerial vehicles. *International Journal of Hydrogen Energy*, 2008. 33(23): p. 7214-7223.
- [20] Fernandes, A., T. Woudstra, and P. Aravind, System simulation and exergy analysis on the use of biomass-derived liquid-hydrogen for SOFC/GT powered aircraft. *International Journal of Hydrogen Energy*, 2015. 40(13): p. 4683-4697.
- [21] Okai, K. et al. Performance analysis of a fuel cell hybrid aviation propulsion system. in *10th International Energy Conversion Engineering Conference*. 2012.
- [22] Okai, K., et al. Investigation of FC/GT hybrid core in electrical propulsion for fan aircraft. in *51st AIAA/SAE/ASEE joint propulsion conference*. 2015.

- [23] Yanovskiy, L.S. et al., Alternative fuels and perspectives solid oxide fuel cells usage in air transport. *ECS Transactions*, 2013. 57(1): p. 149.
- [24] Guo, F. et al., Performance analysis of a turbofan engine integrated with solid oxide fuel cells based on Al-H<sub>2</sub>O hydrogen production for more electric long-endurance UAVs. *Energy Conversion and Management*, 2021. 235: p. 113999.
- [25] Roushenas, R. et al., Thermo-environmental analysis of a novel cogeneration system based on solid oxide fuel cell (SOFC) and compressed air energy storage (CAES) coupled with turbocharger. *Applied Thermal Engineering*, 2020. 181: p. 115978.
- [26] Ji, Z. et al., Advanced exergy and graphical exergy analyses for solid oxide fuel cell turbine-less jet engines. *Journal of Power Sources*, 2020. 456: p. 227979.
- [27] Jansen, R. et al. Turboelectric aircraft drive key performance parameters and functional requirements. in 51st AIAA/SAE/ASEE joint propulsion conference. 2015.
- [28] Roth, B. and R. Giffin. Fuel cell hybrid propulsion challenges and opportunities for commercial aviation. in 46th AIAA/ASME/SAE/ASEE joint propulsion conference & exhibit. 2010.
- [29] Ly, L.T., Computational Investigation and Experimental Validation of a Small Subsonic Turbine-less Jet Engine Concept. 2010, California State University, Los Angeles.
- [30] Buchanan, T., I. Anderson, and S. Woodard, Ultralight Turbine-less Jet Engine. 2016.
- [31] Ji, Z. et al., Performance assessment of a solid oxide fuel cell turbine-less jet hybrid engine integrated with a fan and afterburners. *Aerospace Science and Technology*, 2021. 116: p. 106800.
- [32] Ji, Z. et al., Comparative performance analysis of solid oxide fuel cell turbine-less jet engines for electric propulsion airplanes: Application of alternative fuel. *Aerospace Science and Technology*, 2019. 93: p. 105286.
- [33] Martinez, A.S., J. Brouwer, and G.S. Samuelsen, Comparative analysis of SOFC-GT freight locomotive fueled by natural gas and diesel with onboard reformation. *Applied energy*, 2015. 148: p. 421-438.
- [34] Spallina, V. et al., Integration of solid oxide fuel cell (SOFC) and chemical looping combustion (CLC) for ultra-high efficiency power generation and CO<sub>2</sub> production. *International Journal of Greenhouse Gas Control*, 2018. 71: p. 9-19.
- [35] Xu, Y.-w. et al., Development of solid oxide fuel cell and battery hybrid power generation system. *International Journal of Hydrogen Energy*, 2020. 45(15): p. 8899-8914.
- [36] Marefati, M., M. Mehrpooya, and S.A. Mousavi, Introducing an integrated SOFC, linear Fresnel solar field, Stirling engine and steam turbine combined cooling, heating and power process. *International Journal of Hydrogen Energy*, 2019. 44(57): p. 30256-30279.
- [37] Pirkandi, J., M. Mahmoodi, and M. Ommian, An optimal configuration for a solid oxide fuel cell-gas turbine (SOFC-GT) hybrid system based on thermo-economic modelling. *Journal of Cleaner Production*, 2017. 144: p. 375-386.
- [38] Mehrpooya, M., H. Dehghani, and S.A. Moosavian, Optimal design of solid oxide fuel cell, ammonia-water single effect absorption cycle and Rankine steam cycle hybrid system. *Journal of Power Sources*, 2016. 306: p. 107-123.
- [39] Moradi, M. and M. Mehrpooya, Optimal design and economic analysis of a hybrid solid oxide fuel cell and parabolic solar dish collector, combined cooling, heating and power (CCHP) system used for a large commercial tower. *Energy*, 2017. 130: p. 530-543.
- [40] Siddiqui, O. and I. Dincer, Analysis and performance assessment of a new solar-based multigeneration system integrated with ammonia fuel cell and solid oxide fuel cell-gas turbine combined cycle. *Journal of Power Sources*, 2017. 370: p. 138-154.
- [41] Chan, S., K. Khor, and Z. Xia, A complete polarization model of a solid oxide fuel cell and its sensitivity to the change of cell component thickness. *Journal of power sources*, 2001. 93(1-2): p. 130-140.
- [42] Aguiar, P., C. Adjiman, and N.P. Brandon, Anode-supported intermediate temperature direct internal reforming solid oxide fuel cell. I: model-based steady-state performance. *Journal of power sources*, 2004. 138(1-2): p. 120-136.
- [43] Alaswad, A. et al., Advances in Solid Oxide Fuel Cell Materials, in Reference Module in Materials Science and Materials Engineering. 2020, Elsevier.
- [44] Ali, S., K. Sørensen, and M.P. Nielsen, Modeling a novel combined solid oxide electrolysis cell (SOEC)-Biomass gasification renewable methanol production system. *Renewable Energy*, 2020. 154: p. 1025-1034.
- [45] Ji, Z. et al., Determination of the safe operation zone for a turbine-less and solid oxide fuel cell hybrid electric jet engine on unmanned aerial vehicles. *Energy*, 2020. 202: p. 117532.
- [46] Korakianitis, T. and D. Wilson, Models for predicting the performance of Brayton-cycle engines. 1994.
- [47] Ji, Z. et al., Thermodynamic performance evaluation of a turbine-less jet engine integrated with solid oxide fuel cells for unmanned aerial vehicles. *Applied Thermal Engineering*, 2019. 160: p. 114093.
- [48] Manigandan, S. et al., Impact of additives in Jet-A fuel blends on combustion, emission and exergetic

analysis using a micro-gas turbine engine. *Fuel*, 2020. 276: p. 118104.

[49] Naseri, A. et al., Thermodynamic and Exergy Analyses of a Novel Solar-Powered CO<sub>2</sub> Transcritical Power Cycle with Recovery of Cryogenic LNG Using Stirling Engines. *Renewable Energy Research and Applications*, 2020. 1(2): p. 175-185.

[50] Almeida Pazmiño, G.A. and S. Jung, Thermodynamic modeling of sulfuric acid decomposer integrated with 1 MW tubular SOFC stack for sulfur-based thermochemical hydrogen production. *Energy Conversion and Management*, 2021. 247: p. 114735.

[51] Abbasi, H.R. et al., Thermodynamic analysis of a tri-generation system using SOFC and HDH desalination unit. *International Journal of Hydrogen Energy*, 2021.

[52] Javadi, M.A. et al., Comparison of Monte Carlo Simulation and Genetic Algorithm in Optimal Wind Farm Layout Design in Manjil Site based on Jensen

Model. *Renewable Energy Research and Applications*, 2021. 2(2): p. 211-221.

[53] Ghazvini, M., S.M. Pourkiaei, and F. Pourfayaz, Thermo-Economic Assessment and Optimization of Actual Heat Engine Performance by Implementation of NSGA II. *Renewable Energy Research and Applications*, 2020. 1(2): p. 235-245.

[54] Singh, K. et al., Optimization of tribological performance of natural fibers/epoxy composites using ANOVA & TOPSIS approach. *Materials Today: Proceedings*, 2021.

[55] Mehrpooya, M. et al., Numerical investigation of a new combined energy system includes parabolic dish solar collector, Stirling engine and thermoelectric device. *International Journal of Energy Research*, 2021.

[56] Guler, E. and S. Yerel Kandemir, Assessment of Wind Power Plant Potentials via MCDM Methods in Marmara Region of Turkey. *Renewable Energy Research and Applications*, 2021. 2(2): p. 157-163.